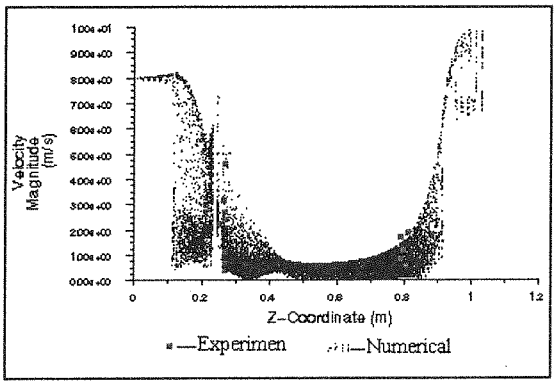

Figure (20) Velocity magnitude distribution along centerline direction (case 2).

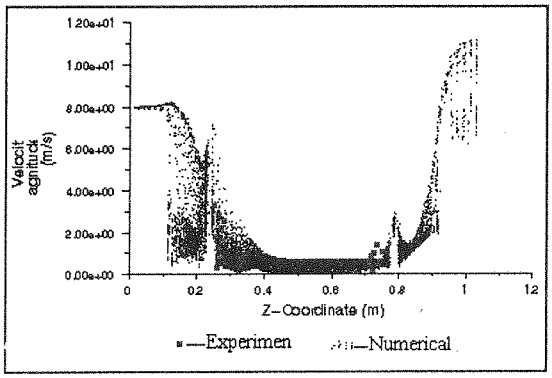

Figure (21) Velocity magnitude distribution along centerline direction (case 3).

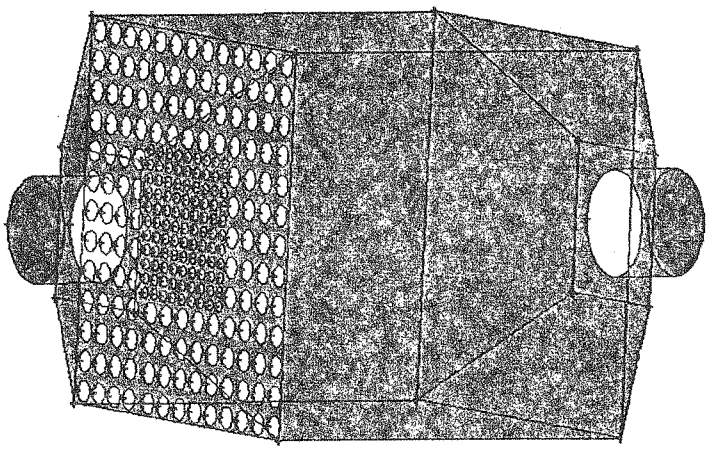

Figure (22) Geometry of electrofilter with a combined distribution plate after inlet duct.

References

[1] G. Ahmadi, and D. H. Smith, Computational Modeling of Particle Transport and Deposition in Hot - Gas Cleanup Filter Vessels - IGCF with Two Filter, 1997.

[2] H.J. White, Industrial electrostatic precipitation, Addison Wesley Inc, 1963.

[3] G. Cooperman, Aunified efficiency theory for electrostatic precipitator, Atoms. Environment. 18,no. 2:277-285, 1984.

[4] M. Crawford, Air pollution control theory , McGraw Hill Inc, 1976.

[5] A. Li, G. Ahmadi., R.G. Bayer and M.A. Gaynes, Aerosol Particle Deposition in an Obstructed Turbulent Duct Flow, J.Aero.sci , vol.25 , pp. 91-112 , 1994.

[6]

[7] H.K. Versteeg & W. Malalasekera, An introduction to computational fluid dynamics The finite volume method , first edition, longman Group ltd,1995.

[8] G. B. Schubauer, W. G. Spangenburg , and P. S. Klebanoff, Aerodynamic Characteristics of Damping Screens, NACA TN 2001, Janury 1950.

[9] P. G. Morgand , The Stability of Flow Thru Porous Screens , JAS 64 , 359, 1960.

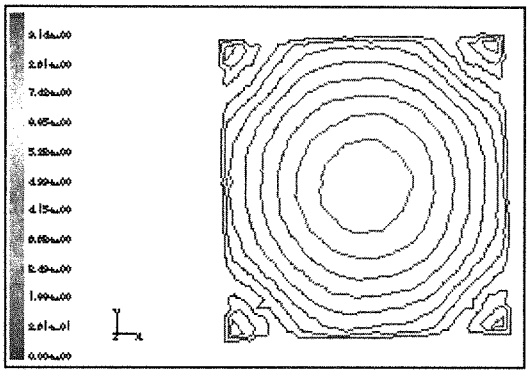

Figure (14) Countors of velocity magnitude in cross-section before outlet distribution plate (case 2).

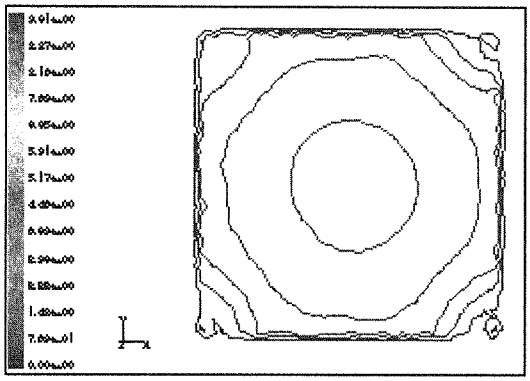

Figure (17) Countors of velocity magnitude in cross-section at mid-poin of electrofilter (case 2).

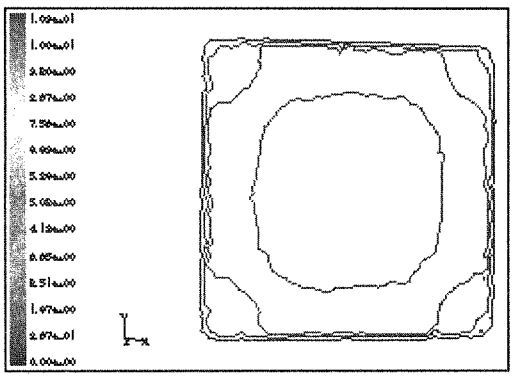

Figure (15) Countors of velocity Magnitude in cross-section before outlet distribution plate (case 3).

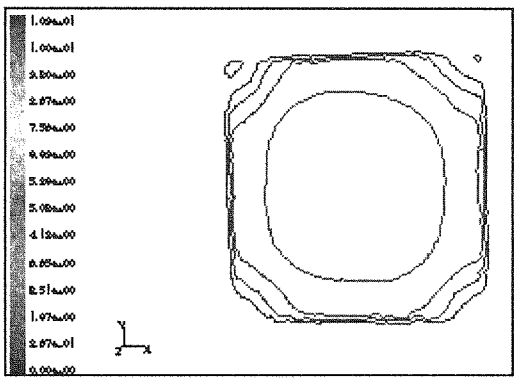

Figure (18) Countors of velocity magnitude in cross-section at mid-poin of electrofilter (case 3).

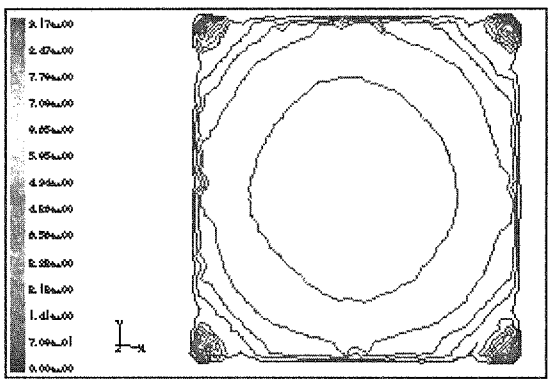

Figure (16) Countors of velocity magnitude in cross-section at mid-poin of electrofilter (case 1).

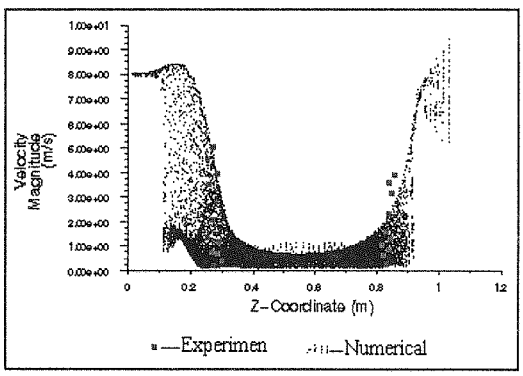

Figure (19) Velocity magnitude distribution along centerline direction (case 1).

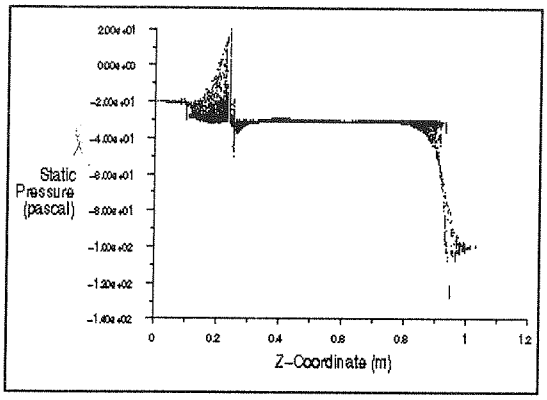

Figure (8) Pressure distribution along centerline direction (case 2).

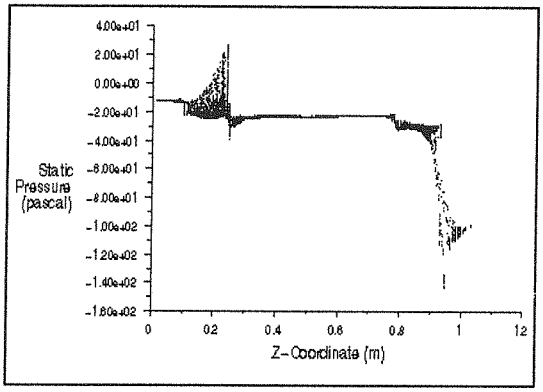

Figure (9) Pressure distribution along centerline direction (case 3).

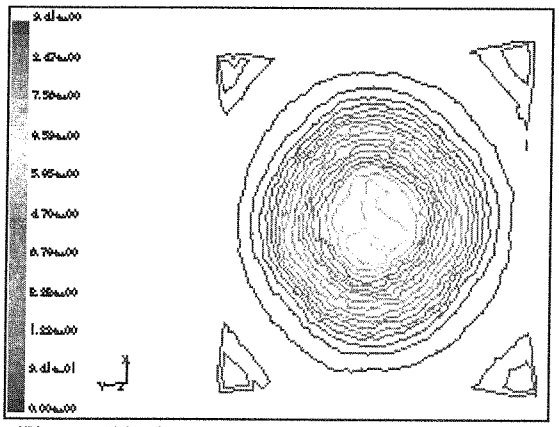

Figure (10) Countors of velocity magnitude in cross-section after inlet distribution plate (case 1).

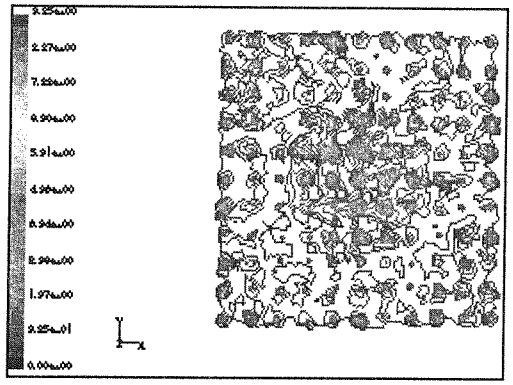

Figure (11) Countors of velocity magnitude in cross-section after inlet distribution plate (case 2).

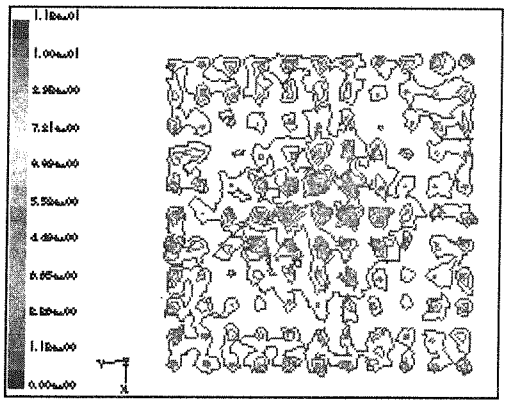

Figure (12) Countors of velocity magnitude in cross-section after inlet distribution plate (case 3).

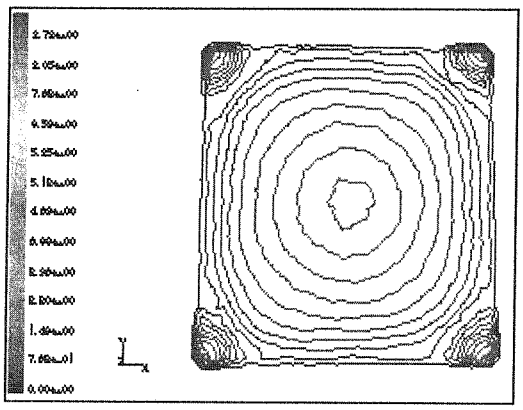

Figure (13) 0 Countors of velocity magnitude in cross-section before outlet distribution plate (case 1).

2. In practice use of non-uniform distribution plate after inlet duct is very efficient, but this matter needs further consideration..
3. We can use these results for wind tunnels, because a uniform distribution of flow is required.
4. As the continues of this research we can use guide blade at inlet duct for uniforming flow distribution.
5. For more prease study of flow inside electrofilter we must apply electrostatic force as a source in the governing equation and start the electrostatic field in device to comparing results.

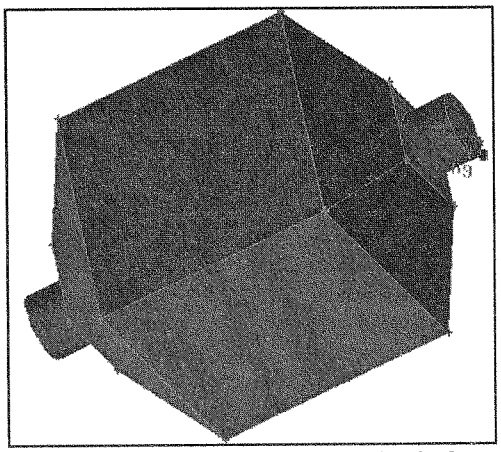

Figure (2) Shematic view of physical domain of computational simulation.

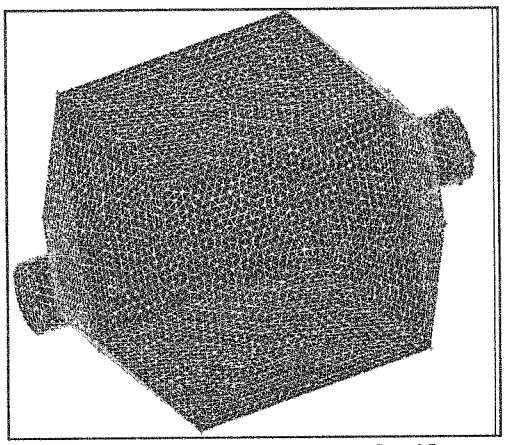

Figure (3) 3-D Unstructured grid generated of physical domain.

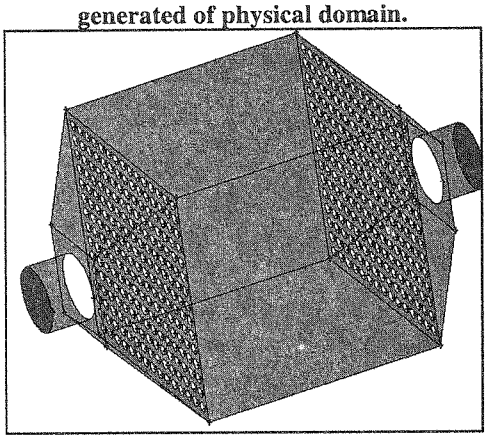

Figure (6) Geometry of case 3.

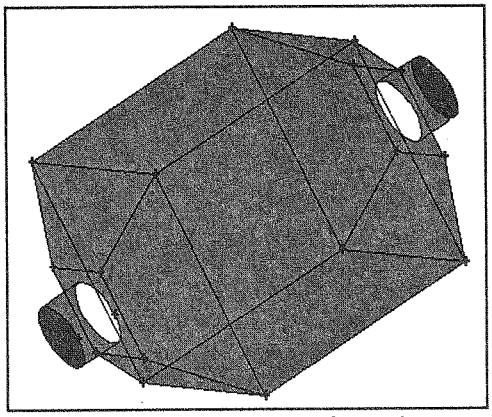

Figure (4) Geometry of case 1.

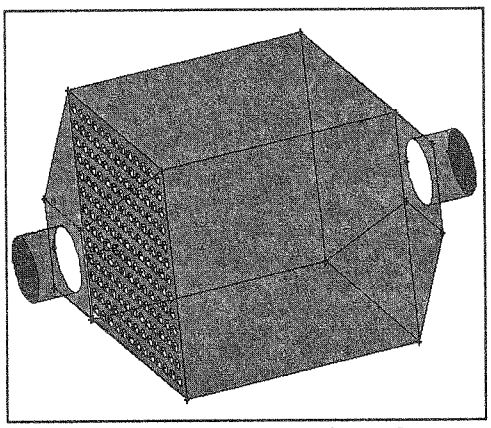

Figure (5) Geometry of case 2.

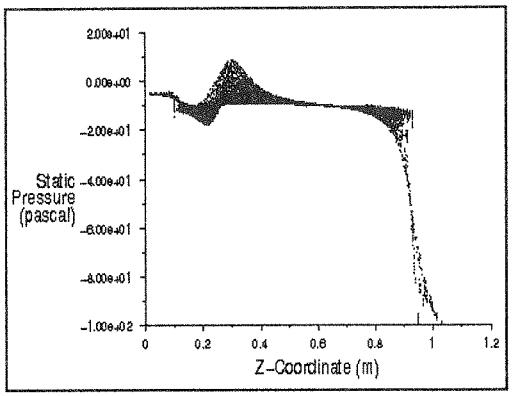

Figure (7) Pressure distribution along centerline direction (case 1).

3: one distribution plate placed after inlet duct and another placed before outlet duct) is shown in figures 4, 5 and 6, respectively. Pressure distribution along symmetry line of filter is shown in figures 7, 8 and 9, for cases 1, 2 and 3, respectively.

Counters of velocity magnitude in cross-section after inlet distribution plates are shown in figures 10, 11 and 12 for case1, case2 and case3 respectively.

Counters of velocity magnitude in cross-section before outlet distribution plates are shown in figures 13, 14 and 15 for case1, case2 and case3 respectively. Counters of velocity magnitude in cross-section at mid-point of electrofilter are shown in figures 16, 17 and 18 for case1, case2 and case3 respectively. Velocity magnitude distribution along symmetry line of filter is shown in figures 19, 20 and 21, for cases 1, 2 and 3, respectively. Figure 22 shows a non-uniform or combined distribution plate after inlet duct.

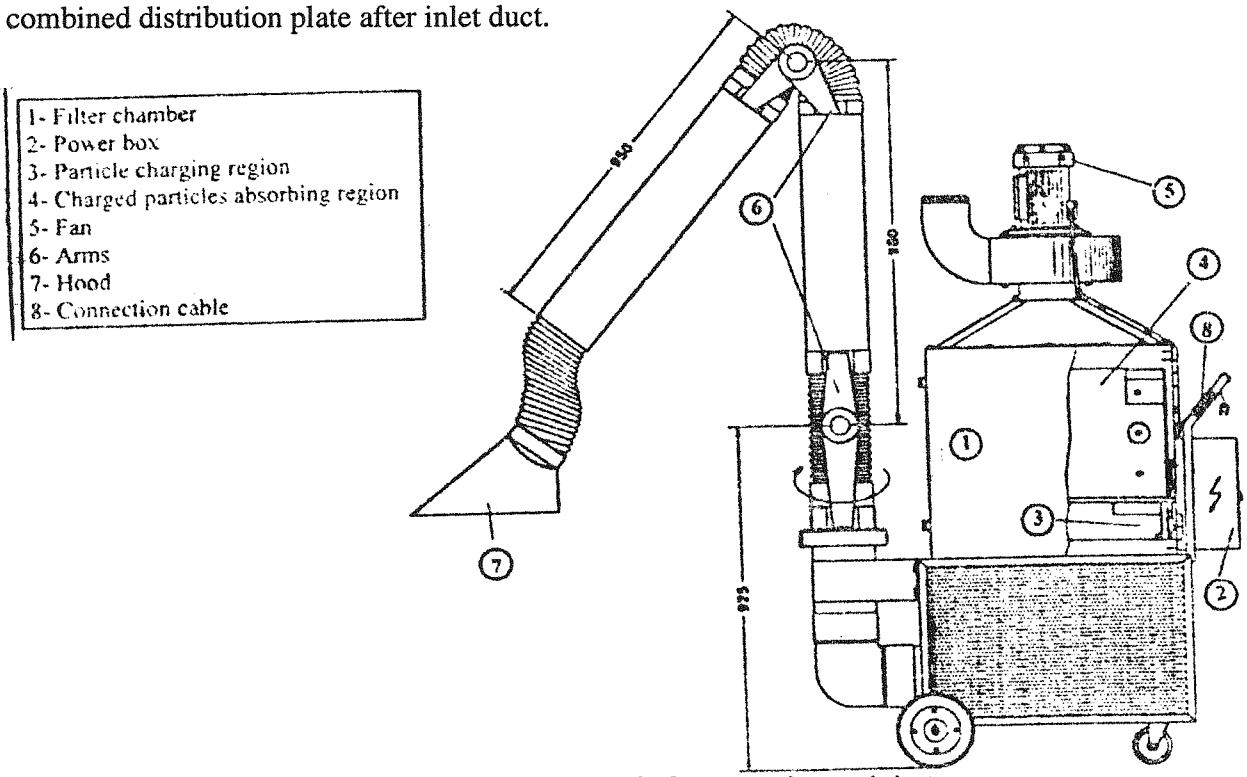

Figure (1) Shematic view of electrostatic precipitator.

Discussion

We can see that sudden reduction of pressure is due suction fan near the outlet boundary in figures 7, 8 and 9. Comparing figures 7, 8 and 9 shows that the distribution of pressure in charging chamber of case 3 more is uniform than two other cases. In these figures, pressure increase near inlet can be due to distribution plate. It is clear by comparing the fissures 10/11 and 12 that the distribution of velocity magnitude after inlet distribytion plate is more uniform than the other two cases. However, we must note an important pointie, if the size of open circles at the center of distribution plate was smaller than the other points, than distribution of velocity magnitude will very uniform than this state..

Figures 13 to 18 show results similar to figures 10 to 12. Figure 21 shows a uniform velocity distribution in charging chambers in compare with the other two cases. Comparing numerical and experimental results in figures 19, 20 and 21 show good agreement. According to this numerical and experimental results:

1. The fluent software is suitable and efficient for simulation of some problems.

$$\beta = \frac{\text{projected open area}}{\text{Total area}} \qquad (15)$$

D = diameter of open circles

R_d = Re ynolds number **based on open diameter , d**

Geometry and Grid generation

Physical domain or geometry is combined from inlet cylinder, inlet duct, charging chamber (a cube 0.5m x 0.5m x 0.5m), outlet duct, outlet cylinder, and two number of models (case2 and case3) have respectively one and two distribution plates (as shown in figures 5 and 6). Diameter of open circles in distribution plates is 7.5mm, and β of distribution plates is 50%(projected open area is 0.25m^2 on total area is $0.5m^2$).

For grid generating we use GAMBIT software (version 1.1), and because complexity of physical domain we apply unstructured grid, with 400000 hedragonal elements (figure3).

Boundary conditions

For numerical solution we use Fluent software (version 5.3). Inlet boundary defined as Velocity magnitude 8m/s, turbulence intensity 4% and turbulence length scale 0.03m. The exit boundary defined as constant pressure -100 Pascal (there is a suction fan) and the same turbulence quantities. Numerical solution converged after 500 iterations with 10^{-4} accurate. To define wall boundary condition applied non-zero condition.

Viscosity and density of fluid flow is respectively $1.7\times10^{-5}\ \text{N.s/m}^2$ and $1.17\ \text{kg/m}^3$.

Experimental investigation

Experimental setup is shown in figure1. It contains filter chamber (inlet duct, main chamber and outlet duct), power box, particle charging chamber, charged particles absorbing chamber, fan, arms, hood and connection cable.

In experimental tests, using a testo-445 measuring instrument the flow velocity was measured at inlet and outlet zone (after inlet duct and before outlet duct) of electrostatic precipitator. The probe used for performing these tests was a Pitot tube with 0.5 lengths. For these reasons air velocity was measured in three tests as below:

Case1: Electrostatic precipitator without distribution screen.

Case2: Electrostatic precipitator with distribution screen at inlet zone (after inlet duct or before charging chamber).

Case3: Electrostatic precipitator with distribution screens at inlet and outlet zones (once before charging chamber and other is placed after charging chamber).

Experimental results of case1, 2 and three compared with numerical results and shown in figures 19, 20 and 21, respectively.

Results

The schematic view of electrostatic precipitator is shown in figure1. Figure2 show Physical domain of computational simulation. Figure3 shows 3-D unstructured grid in physical domain that is produced in Gambit software with 400000 tetragonal elements. Geometry of physical domain for three cases (1: without any distribution plate, 2: one distribution plate after inlet duct,

$$\nu_{eff} = \nu_{mol}\left[1+\sqrt{\frac{C_\mu}{\nu_{mol}}}\frac{k}{\sqrt{\varepsilon}}\right]^2 \tag{8}$$

The transport equations for k and ε in the RNG model are [6]:

$$\frac{\partial k}{\partial t}+u_i\frac{\partial k}{\partial x_i}=\nu_t S^2-\varepsilon+\frac{\partial}{\partial x_i}\alpha\nu_t\frac{\partial k}{\partial x_i} \tag{9}$$

And

$$\frac{\partial \varepsilon}{\partial t}+u_i\frac{\partial \varepsilon}{\partial x_i}=C_{1\varepsilon}\frac{\varepsilon}{k}\nu_t S^2-C_{2\varepsilon}\frac{\varepsilon^2}{k}-R+\frac{\partial}{\partial x_i}\alpha\nu_t\frac{\partial \varepsilon}{\partial x_i} \tag{10}$$

Where α is the inverse prandtl number for turbulent transport. The rate-of-strain term R is given by:

$$R=2\nu_{mol}S_{ij}\overline{\frac{\partial u_k'}{\partial x_i}\frac{\partial u_k'}{\partial x_j}} \tag{11}$$

This term is expressed in the RNG $k-\varepsilon$ model equations as:

$$R=\frac{C_\mu\eta^3(1-\eta/\eta_\circ)}{1+\beta\eta^3}\frac{\varepsilon^2}{k} \tag{12}$$

Where $\eta=Sk/\varepsilon$, $\eta_\circ\approx 4.38$, and $S^2=2S_{ij}S_{ij}$ is the modulus of the rate of strain tensor. The RNG theory gives value of the constants $C_{1\varepsilon}=1.42$ and $C_{2\varepsilon}=1.68$, and $\alpha=1.39$.

Effect of distribution Plates (Screens)

Turbulence in the inlet section is reduced by the installation of screen. Screens reduce the axial turbulence more than the lateral turbulence [9]. Screens have a relatively large pressure drop in the flow direction, which reduces the higher velocities more than the lower, and thus promote a more uniform axial velocity. For screens, many of the turbulent reduction theories are based on a pressure loss coefficient K, defined as pressure loss across the screen ΔP divided by the mean flow dynamic pressure. Therefore [8]:

$$K=K_\circ+\frac{55.2}{R_d} \tag{13}$$

Where

$$K_\circ=\left(\frac{1-0.95\beta}{0.95\beta}\right)^2 \tag{14}$$

whose energy spectrum follows the famous Kolmogorov law $E(k) = k^{-5/3}$. The importance of the RNG approach is that once the inertial range eddies can be accounted for in a quantitatively correct way, we may then obtain coarse-grained equations of motion for the other relevant variables of the turbulence, including the mean velocity, rms velocities, etc. Turbulent flows have eddies that range in size from so-
down to eddies size $L/Re^{3/4}$, where $Re = v_{rms}L/\nu$ is the Reynolds number. Still smaller eddies exist, but they have exceedingly low energy due to viscous dissipation. Thus, accurate solution of the three dimensional Navier-Stokes equations for a turbulent flow require storage of order $O(Re^{9/4})$ and computational work of order $O(Re^3)$ (since turbulence also has a range of time scales of order $Re^{3/4}$). If Re is large, these computational requirements are enormous. RNG methods reduce this computational requirement by eliminating the inertial-range eddies from the equations of motion, yielding equations for averaged flow quantities at the integral scale of the turbulence.

RNG theory develops an equation for the variation of effective viscosity with Reynolds number, which is of the form [6]:

$$\frac{d\nu}{d\ell} = \frac{A\varepsilon\ell^3}{\nu(\ell)^2} \tag{4}$$

Where A is a constant derived by RNG theory.

Integration of Equation 4 over the eddy length scale ℓ, noting that $\nu = \nu_{mol}$ when $\ell = \ell_d$ (where ℓ_d is the Kolomogrov dissipation scale $L/Re^{3/4}$), gives:

$$\nu(\ell) = \nu_{mol}\left[1 + \frac{3A\varepsilon}{4\nu_{mol}^3}\left(\ell^4 - \ell_d^4\right)\right]^{1/3} \quad \ell \geq \ell_d \tag{5}$$

Equation 5 gives an interpolation formula for $\nu(\ell)$ between the molecular viscosity ν_{mol} valid at dissipation scales and the high-Reynolds-number limit of $L \gg \ell_d$. In this high-Reynolds-number limit it can be shown that Equation 5 gives:

$$\nu \approx \nu_t = [0.09L]^2\left|\nabla\bar{u}\right| \tag{6}$$

Where ν_t is the turbulent viscosity ($\nu_{eff} - \nu_{mol}$
classical mixing length theory (which was derived originally as a semi-empirical fit to experimental data). Noting that the total kinetic energy contained in the inertial range eddies of scale less than L is $k = 0.71\varepsilon^{2/3}L^{2/3}$, equation 6 becomes:

$$\nu_t = C_\mu\frac{k^2}{\varepsilon} \qquad \text{With } C_\mu = 0.0845 \tag{7}$$

The result is a differential relationship between ν_{eff} and $k/\sqrt{\varepsilon}$; a simplified algebraic form of the relationship is given below:

from the screen is turbulent, but this is a small-scale turbulence, it quickly damps out. The effects of distribution plates or screens in wind tunnels were reported experimentally in References [8] and [9].

In the present work, a computational modelling study of air flow in a mobile (pilot-scale) electrostatic precipitator (ESP) with three different combined distribution plates is performed and the effect of distribution plates for informing velocity distribution in every section of filter considered. The *RNG* $k-\varepsilon$ turbulence model of the FLUENT code is used for simulating the mean flow velocity in the filter [6], [7]. Then, numerical results compared with results of pitot-tube meassuring. Finally, by considering the results of three cases a new model is recommended, that has a non-uniform distribution plate after inlet duct with smaller open circles at center and larger open circles at around. The other research in this field can be about distribution blades, inlet and outlet ducts and etc.

Computational simulation

The basic equations describing the laminar flow of continuous fluid are [7]:

Conservation of mass or continuity equation is:

$$\frac{\partial \rho}{\partial t}+\frac{\partial}{\partial x_i}(\rho u_i) \tag{1}$$

Conservation of momentum in the i direction in an inertial reference frame, is:

$$\frac{\partial}{\partial t}(\rho u_i)+\frac{\partial}{\partial x_j}(\rho u_i u_j)=-\frac{\partial p}{\partial x_i}+\frac{\partial \tau_{ij}}{\partial x_j}+\rho g_i+F_i \tag{2}$$

Where p is the static pressure, τ_{ij} is the stress tensor, and g_i and F_i are gravitational acceleration and external body forces (e.g. that arising from interaction from interaction with the electrostatic force) in the I direction, respectively.

The stress τ_{ij} is given by:

$$\tau_{ij}=\left[\mu\left(\frac{\partial u_i}{\partial x_j}+\frac{\partial u_j}{\partial x_i}\right)\right]-\frac{2}{3}\mu\frac{\partial u_k}{\partial x_k}\delta_{ij} \tag{3}$$

Where μ is the molecular viscosity and the second term on the right hand side is the effect of volume dilation.

Turbulence modelling

Modeling of turbulent flows requires appropriate modeling procedures to describe the effects of turbulent fluctuations of velocity and scalar quantities on the basic conservation equations. In this investigation to modeling turbulence we use RNG $k-\varepsilon$ model. The RNG $k-\varepsilon$ turbulence model follows the two-equation turbulence-modeling framework and has been derived from the original governing equations for fluid flow using mathematical techniques called Renormalization Group (RNG) methods. The RNG method gives a theory of the Kolmogorov equilibrium range of turbulence, comprising the so-called inertial range of small-scale eddies

Experimental & Numerical Simulation the Effect of Distribution Plates in a Mobile Electrostatic Precipitator

A. R. Noorpoor
MSc.

M. Sadeghi
MSc.

Electrostatic Precipitator Research Center of Jahad Daneshgahi
Iran University of Science and Technology (IUST)

Abstract

In this investigation, behaviour of airflow inside an electrostatic precipitator with three different distribution plates has been considered by means of numerical & experimental methods and results have been compared together. This device has been designed & produced in this center for the first time in Iran, and its ability to absorb particles, haze and soot is good. But for increasing the efficiency there must be some changes to on miscellaneous sections. Therefore, here we consider the effect of distribution plates to increase performance, because when distribution flow at cross sections of precipitator is uniform, the efficiency will increase. To have a numerical simulation, fluent software version 5.3 was used, and for modelling turbulence the RNG $k-\varepsilon$ ***turbulent model applied. This program after discretization governing equations on a body fitted coordinate system, that is produced in preprocessor, integrates this equations on control volumes and determines the rate of quantities on control volume faces using order two (upwind) approximations. Finally by means of a Pitot tube velocity magnitude of fluid in two sections of domain was measured & compared with numerical results which shows a good agreement.***

After simulation the three model, e.g. without distribution plate, with a distribution plate after inlet duct and with two distribution plates (once after inlet duct and other before outlet duct), and taking some results and by comparing them, we conclude that the use of combined distribution plate can give a good result.

Keywords

Computational Fluid Dynamics, Electrostatic Precipitator, Turbulence, Distribution Plate

Introduction

Electrostatic precipitation uses the forces of an electric field on electrically charged particles to separate solid or liquid aerosols from a gas stream [1]. The aerosol is deliberately charged and passed through an electric field causing the particles to migrate towards an opposite charged electrode, which acts as a collection surface. Gravity or rapping the collector electrode removes the particles from the precipitator. Various physical configurations are used in the charging, collection, and removal processes [2].

ESP's are characterized by high efficiencies, even for small particles. They can handle large gas volumes with low-pressure drops and can be designed for a range of temperatures. On the other hand, they involve high capital costs, take up a lot of space, and are not flexible after installation to changes in operating conditions. They may not work on particles with high electrical resistivity [3], [4]. Turbulence in the charging chamber of filter is reduced by the installation of screen after inlet duct. Screen reduces the axial turbulence more than the lateral turbulence. Screens have a relatively large pressure drop in the flow direction which reduces the higher velocities more than the lower, and thus promote a more uniform axial velocity. The wake